Optical properties of conjugated hydrophobic weak polyelectrolytes: Effects of pH, temperature and ionic strength

F. Schosseler, P. Vallat, N. Kutsevol, J.-M. Catala & M. Rawiso

Published online: 14 Dec 2016.

Submit your article to this journal

Article views: 4

View related articles

View Crossmark data

Taylor & Francis
Taylor & Francis Group

Optical properties of conjugated hydrophobic weak polyelectrolytes: Effects of pH, temperature and ionic strength

F. Schosseler[a], P. Vallat[a], N. Kutsevol[b], J.-M. Catala[a], and M. Rawiso[a]

[a]Université de Strasbourg, Institut Charles Sadron, Strasbourg, France; [b]Faculty of Chemistry, National Taras Shevchenko University, Kyiv, Ukraine

ABSTRACT

We measure the UV-visible absorption of an annealed hydrophobic conjugated polyelectrolyte as a function of the pH, for different temperatures and ionic strengths. The position of the absorption maximum shifts non-monotonically as the neutralization degree f decreases from 1 to 0, thus defining two regimes. In the hydrophilic regime, $1 > f > f_1$, the red shift is due to dominant direct Coulombic interactions between the charges along the backbone and the ? electrons, without significant conformational effects. In the hydrophobic regime, $f_1 > f > 0$, the blue shift is dominated by conformational effects with two successive isosbestic points as f decreases. We propose two possible scenarios for the collapse of the chains at low neutralization degrees.

1. Introduction

Substituting conjugated polymer backbones with ionizable groups was proven a convenient method to solubilize conjugated polymers in aqueous solutions a long time ago [1, 2]. Recently these water-soluble compounds allowed a breakthrough for promising applications in the field of sophisticated biosensing techniques [3, 4, 5, 6]. In this context, understanding the optical response of conjugated polyelectrolytes in varying aqueous solution conditions has become an important issue for the design of sensors with enhanced sensitivity [7, 8, 9, 10].

The delocalization of π electrons along the backbone of a conjugated polymer is limited by imperfect overlap of the $2p$ orbitals resulting in particular from either static defects, like regio-randomness, or dynamic bending and twisting fluctuations in the backbone configurations [11]. Therefore the optical properties of conjugated polymers in solution reflect the intrinsic conformational disorder of flexible or semi-flexible polymer chains: an average extended conformation of the chains is expected to be statistically associated with local monomer configurations that allow a better overlap of the $2p$ orbitals than in the case of collapsed chains.

Like most polyelectrolytes, conjugated polyelectrolytes have a hydrophobic backbone and their average conformation in aqueous solutions results from the balance of multiple interactions, e.g., hydrophobic and van der Waals interactions, hydrogen bonding, steric and coulombic repulsions. Moreover the presence of charged groups can a priori be responsible for two opposite trends: while the stretching of the chains by electrostatic repulsions is expected to delocalize the π electrons, the presence of electrostatic potential wells along the

backbone could localize them. Therefore understanding the optical behavior of conjugated polyelectrolytes as a function of, e.g., their degree of ionization or the ionic strength of the solution appears as an intricate problem.

In this paper we take a first step to addressing it by measuring the UV-visible absorption of a conjugated weak polyacid as a function of neutralization degree in the presence of varying added salt concentration. More specifically we titrate very dilute solutions of poly(3-thiophene sodium acetate) with chlorhydric acid and measure simultaneously the pH and the absorption spectra. We are then able to distinguish two regimes of neutralization degrees according to whether the optical properties are dominated by the direct effect of Coulombic interactions between π electrons and charged side groups or by conformational effects (indirect effect of Coulombic interactions).

2. Experimental

2.1. Samples

The synthesis, the fractionation and the characterization of the polymers have been described elsewhere [12, 13]. The poly(3-thiophene acetic acid) (P3TAA) is obtained through saponification of the ester groups of poly(thiophene-3-methyl acetate) (P3TMA) chains, first synthesized by an oxidative-coupling polymerization [14, 15], as proposed by Kim et al. [16]. In this work we used two fractions with number-averaged degree of polymerization $N = 45$ (M_w/M_n = 1.5) and $N = 125$ ($M_w/M_n = 2.2$) with moderate size polydispersity. ^{1}H and ^{13}C NMR analysis showed that the samples can be considered as non-regioregular [13]. The solutions were prepared by weighing the appropriate amount of polymer in ultra pure water (Millipore) for titration experiments or in D$_2$O (Eurisotop, 99.9%) for neutron scattering experiments. They were heated at 50°C for two hours and prepared least two days before use.

2.2. Titration and UV-visible absorption spectroscopy

The back titration of the polysalt (P3TNaA) in a slight excess of NaOH has been chosen because it allows a better molecular dispersion of the chains than the direct titration of the polyacid [13]. The thermally regulated dilute polymer solution (1.6 mM) is titrated by adding 0.1 mL of a 20 mM HCl solution in 2.5 min time steps. At the end of each step, the pH value and a UV-visible absorption spectrum ($300 < \lambda$ (nm) < 800) are recorded. The pH value is measured with a Mettler Toledo pH-meter (MA235) and a gel-containing electrode (Inlab 417).

Long conjugated chains have the electronic structure of semiconductors with an energy gap $E_g \geq 1eV$. Therefore the spectrum of transitions across the gap can be directly probed by UV-visible absorption spectroscopy (UVVAS). Due to the static and dynamic disorder associated with the structure and the conformation of conjugated polymers the absorption spectrum $\varepsilon(\lambda)$ is broad with usually one peak at $\lambda_{max} \sim E_g^{-1}$. The integrated absorption coefficient is [17]:

$$\bar{\varepsilon} = \int \varepsilon(\lambda)d\lambda \propto \sum_{i,f} F_{if} \propto \sum_{i,f} (E_f - E_i)\big|< f\,|\mathbf{P}|\,i >\big|^2 \qquad (1)$$

where F_{if} is the oscillator strength of the transition between states i and f with energies E_i and E_f, and $\mathbf{P}$ is the dipolar moment of the chain. Eq. (1) can be approximated as $\bar{\varepsilon} \propto \mu^2/\lambda_{max}$

where $\mu^2 = \sum_{i,f} |< f|\mathbf{P}|i >|^2$ is an integrated dipolar moment of transition of the conjugated chain. Chain extension is associated with a reduced conformational disorder and usually a better overlap of the $2p$ orbitals, i.e., with a smaller gap and a larger polarizability. The corresponding increases in λ_{max} and μ^2 can be directly measured in dilute solutions by UVVAS. Therefore there is a direct correlation between the conformation of conjugated polymers and their UV-visible absorption spectrum [18, 19, 20]. The UVVAS is performed with a Varian Cary 50 Scan spectrophotometer equipped with a Hellma immersion probe (1 mm optical path). The low concentration of the samples and the small optical path ensure that the optical density remains smaller than unity in all experiments. Reverse titration by NaOH with the same protocol yields satisfactorily superposing titration curves [13] showing negligible effects of the dilution and of the slight variation in ionic strength during the titration. However in presence of larger than 0.1 M added NaCl, the occurrence of polymer precipitation is noticed for small neutralization degree of the polyacid chains. These effects will be discussed below. Here we define the neutralization degree f as the molar ratio of monomers in the salt form to the total number of monomers.

3. Results

3.1. General features of the absorption spectra

Figure 1 shows the non-monotonic evolution of typical absorption spectra upon HCl addition in the absence of added salt and Figure 2 the corresponding pH and position of the absorption maximum λ_{max}. At the beginning of HCl addition only the slight excess of NaOH is titrated. The titration of the polysalt begins when λ_{max} starts increasing up to a maximum at $f = f_1$ (red shift of the spectra). Then λ_{max} decreases until $f = 0$ (blue shift) down to a value ≈ 399 nm smaller than the initial value ≈ 435 nm. When the evolution of pH reflects merely the further addition of HCl the λ_{max} value stays constant. During the titration between $f = 1$ and $f = 0$, $\bar{\varepsilon}$ is continuously decreasing but μ^2 has the same non-monotonic variation as λ_{max}.
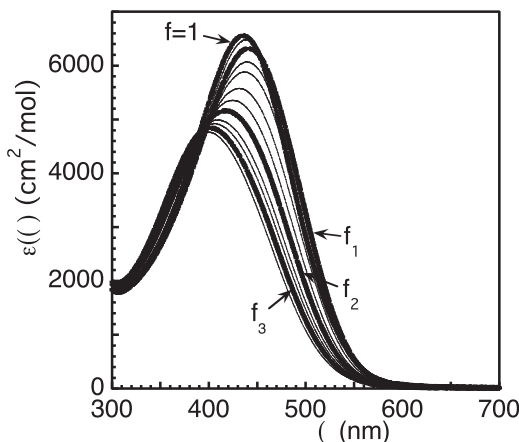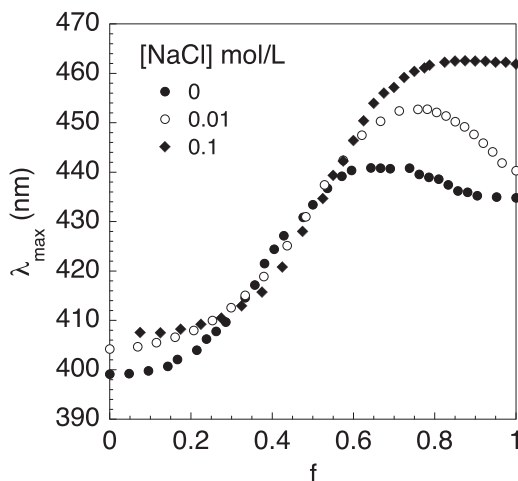

Figure 1. UV-visible absorption spectra during the titration of P3TNaA ($N = 125$) with HCl in the absence of added salt. The thick curves labeled f_i delimit the regimes discussed in the text: f_1, transition between the hydrophilic and hydrophobic regimes; $f_1 > f > f_2$, first isosbestic point; $f_2 > f > f_3$, second isosbestic point (see text).
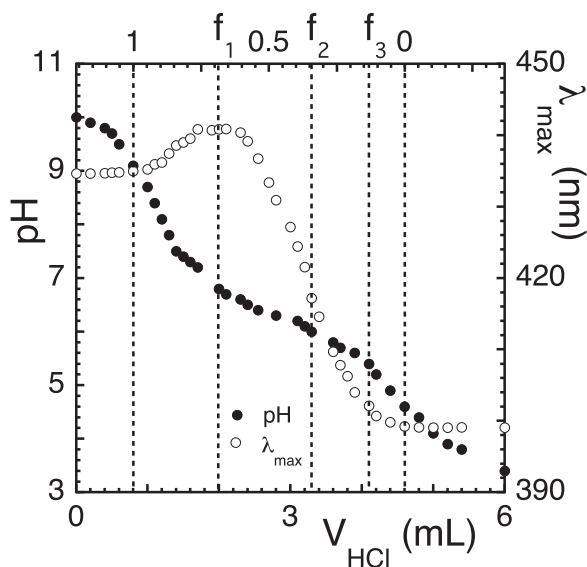
Figure 2. Compared evolutions of pH and λ_{max} during a titration ($N = 125$), as a function of titrant volume (bottom x-axis) and of the corresponding neutralization degree (top x-axis). The maximum value of λ_{max} defines f_1 that marks the limit between the hydrophilic ($f > f_1$) and hydrophobic regimes ($f < f_1$).

These features are modified by the presence of added NaCl in the titration bath as shown by Figure 3. At small ($f \leq 0.25$) and large ($f \geq 0.65$) neutralization degrees the presence of added salt increases the value of λ_{max}. More strikingly, the position of the maximum of $\lambda_{max}(f)$ shifts to higher f values as NaCl concentration increases and finally $\lambda_{max}(f)$ increases monotonically when $C_{NaCl} \geq 0.1$M.

Recent SANS experiments [13] have shown that semidilute solutions of P3TNaA at full neutralization $f = 1$ exhibit the same structure as those of saturated polyelectrolytes like polystyrene sodium sulfonate. In particular, this structure is described by the scaling laws of the isotropic model of semidilute polyelectrolyte solutions [21] and no indication of an aggregation induced by the addition of salt could be found [13]. On the other hand due to its

Figure 3. Influence of added salt on the red and blue shifts of the absorption spectra during titration.

Table 1. Influence of the counterion size on the absorption spectra.

Sample	λ_{max} (nm)	μ^2 (a.u.)
P3TLiA	443	49.5
P3TNaA	442	48.3
P3TKA	444	50.1
P3TCsA	448	48.8

conjugated backbone the unneutralized P3TAA has a poor solubility in pure water and even precipitates in the presence of added salt ($C_{NaCl} \geq 0.1$ M). Therefore the polymer is globally hydrophilic at high f values and globally hydrophobic at small f values. We shall argue in the following that the transition between these two behaviors occurs at $f = f_1$, i.e., when λ_{max} is maximum, and that the variation of λ_{max} with neutralization degree in these two regimes is dominated by different effects.

3.2. The hydrophilic regime $f > f_1$

#### a. Effect of the size of the counterions

We have changed the counterion size by fully neutralizing P3TAA chains with LiOH, NaOH, KOH and CsOH, thus varying the ionic radius of the counterion from about 0.75 to 1.7 Å [22]. As shown by Table 1, in this range the size of the counterion has no influence on the position of the absorption maximum within the experimental accuracy. This effect is strikingly different from the behavior reported for regioregular poly(thiophene-3-propionic acid) where a blue shift of 40 nm was observed when the Li$^+$ counterion was replaced by Cs$^+$ [23]. This shift was explained by the strong aggregation of regioregular poly(thiophene-3-propionic acid) that was disrupted by the insertion of the counterion into the aggregates. The absence of such an effect in our solutions shows that such aggregation is not a dominant effect for these regiorandom samples.

b. Effect of the ionic strength

Figure 4 shows the effect of ionic strength on the evolution of λ_{max} of fully neutralized P3TNaA chains. No precipitation of the chains is observed whatever the concentration of added salt in
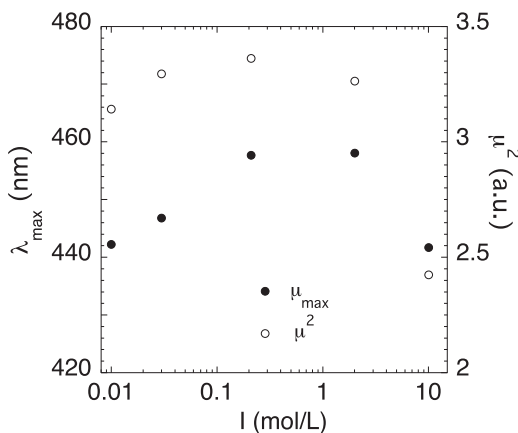
Figure 4. Influence of added NaCl on the position of absorption maximum and on the integrated dipolar moment of transition of P3TNaA ($N = 125$, $f = 1$, 1.6 mM). The ionic strength value I includes the contribution from the counterions of the polymer chains.
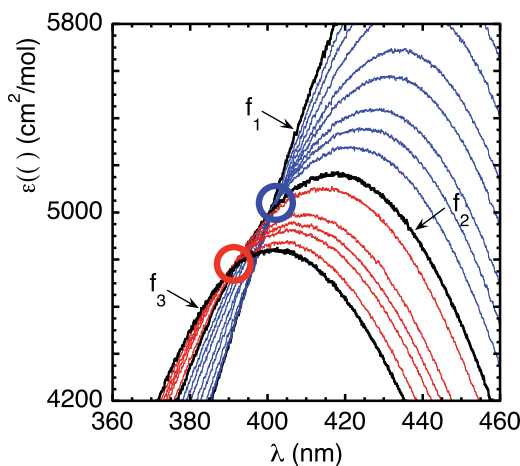
Figure 5. (color online) Zoom in the data of Figure 1 showing the two isosbestic points in the absorption spectra. All spectra for $f_1 \geq f \geq f_2$ (resp. $f_2 \geq f \geq f_3$) intersect in the same point circled in blue at $\lambda \approx 401$ nm (resp. in red at $\lambda \approx 392$ nm).

the range investigated. Up to a salt concentration about 0.2 M, the spectra exhibit a red shift followed by a blue shift at higher salt concentration. The evolution of μ^2 follows the same non-monotonic behavior. While the decrease of λ_{max} and μ^2 at high salt concentration can be understood by the collapse of the chains resulting in a smaller conjugation length, their initial increase upon salt addition is unexpected. The same behavior is observed when adding XCl salts in solutions of P3TXA with X = Li, K or Cs. In the Discussion, we shall argue that the initial increase of λ_{max} is due to the interplay of electrostatic interactions between π electrons, charged groups and condensed counterions.

3.3. The hydrophobic regime $f < f_1$

One striking feature in Fig. 1 (see Fig. 5) is the presence of two isosbestic points (IP) where $\varepsilon(\lambda \approx 401$ nm; $f)$ (resp. $\varepsilon(\lambda \approx 392$ nm; $f))$ is constant for $f_1 \geq f \geq f_2$ (resp. $f_2 \geq f \geq f_3$). An IP is generally associated with an equilibrium between two coexistent species with a conserved total concentration. Only few studies have reported in detail on the pH dependence of the photophysical properties of annealed CPE [1, 16, 27, 28, 29] and the existence of an IP upon pH variation was observed in only two cases [27, 29] as far as we know. For poly(phenylene ethynylene) bearing phosphonate side groups, the red shift in the absorption spectra upon decreasing the neutralization degree was attributed to the increase prevalence of chain aggregation as the charge of the chains decreases [27]. For poly(phenylene vinylene) with pendant acetate ammonium groups, a similar red shift was observed for decreasing ionization degrees and it was attributed to the decreasing twist of the backbone conformation as the electrostatic repulsion between charged groups decreases [29]. Strikingly, in the case of P3TNaA, the opposite trend is observed [12, 16, 30] with a blue shift of the absorption spectra upon decreasing the ionization degree.

The existence of two IP hints at the coexistence in the titration bath of two different electronic states of the chains in each of the ranges $f_1 \geq f \geq f_2$ and $f_2 \geq f \geq f_3$. Here we propose a quantitative analysis to determine the molar fraction of polymer in each state [12, 30]. Indeed
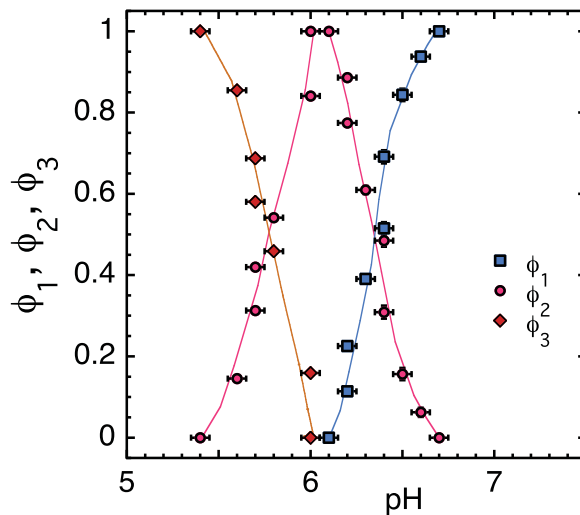
Figure 6. (color online) Variations of Φ_1 (squares), Φ_2 (circles) and Φ_3 (diamonds) with the *pH* for $N = 125$. Error bars correspond to 0.05 pH unit and to the standard deviation of Φ_i values calculated on the interval $400 < \lambda$ (nm) < 500. Lines are guides for the eye.

for each IP any absorption curve in the range $f_i > f > f_j$ can be decomposed as a linear combination of the spectra at f_i and f_j,

$$\varepsilon(\lambda, f) = \Phi_j(f)\varepsilon(\lambda, f_j) + \left[1 - \Phi_j(f)\right]\varepsilon(\lambda, f_i) \tag{2}$$

where $\Phi_j(f)$ represents the molar fraction of monomers in the state associated with $f = f_j$.

Typical relative deviations between the experimental data and the linear combination based on $\varepsilon(\lambda, f_i)$ and $\varepsilon(\lambda, f_j)$, Eq. 2, remain smaller than 0.05 on the right side of the maximum, i.e., in the range $400 < \lambda$ (nm) < 500. Figure 6 shows the complete variations of the Φ_i as a function of pH (no added salt) for the longest chains. Figure 7 shows the variations of Φ_2
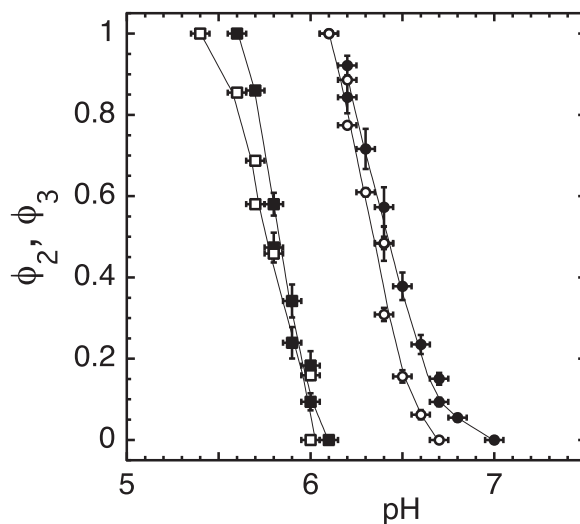
Figure 7. Variations of Φ_2 (circles) and Φ_3 (squares) with the *pH* for different chain lengths: $N = 125$ (open symbols) and $N = 45$ (closed symbols). Error bars and lines as in Fig. 6. For the sake of clarity, $\Phi_1 = 1 - \Phi_2$ and the lower pH part of $\Phi_2 = 1 - \Phi_3$ are not displayed.
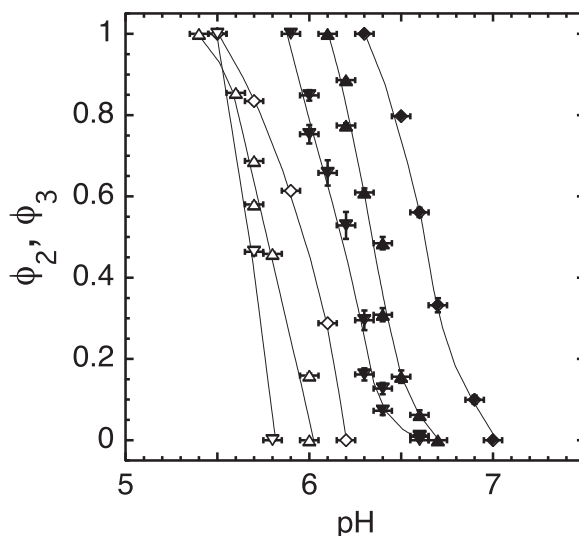
Figure 8. Variations of Φ_2 (closed symbols) and Φ_3 (open symbols) with the *pH* for different temperatures in the absence of added salt: diamonds, 2°C; up triangles, 20°C; down triangles, 70°C. Error bars and lines as in Figure 6. For the sake of clarity, $\Phi_1 = 1 - \Phi_2$ and the lower pH part of $\Phi_2 = 1 - \Phi_3$ are not displayed.

and Φ_3 as a function of pH for the two chain lengths investigated in this paper. For the sake of clarity of the figure, Φ_1 ($= 1 - \Phi_2$) and lower pH Φ_2 ($= 1 - \Phi_3$) data are not displayed. Figure 8 shows similar data when varying the temperature for $N = 125$. Table 2 gives the values of the f_i determined for different molecular weights, temperatures or salt concentrations.

In the Discussion, we shall argue that the features displayed by Figs. 7–8 can be explained by conformational changes of the polymer chains. For the sake of brevity we shall use the term transition i-j for the phenomenon occurring in the range $f_i > f > f_j$.

4. Discussion and conclusions

4.1. The hydrophilic regime f > f₁

Previous SANS experiments have shown that P3TNaA chains behave like hydrophilic polyelectrolytes when $f = 1$ [13]. We notice here that f_1 is larger than the Manning-Oosawa condensation threshold $f_{MO} = b/l_B \approx 0.54$, where $b \approx 3.8$ Å is the monomer length [31] and $l_B = 7.1$ Å is Bjerrum's length. In these conditions the effective charge along the backbone keeps a constant value [32, 33] and no significant change of the chain conformation with f is expected

Table 2. Values of the ionization degrees delimiting the various regimes in the titration for different experimental conditions. Error values are given only for f_2 but are representative of the errors on all f_i due to the discrete sampling of spectra.

N	C_{NaCl} (mol/L)	T°C	f_1	f_2	f_3
45	0	20	0.81	0.49 ± 0.01	0.14
125	0	2	0.79	0.50 ± 0.03	0.26
125	0	20	0.67	0.35 ± 0.03	0.13
125	0	70	0.72	0.30 ± 0.02	0.21
125	0.01	20	0.71	0.41 ± 0.03	0.16
125	0.1	20	0.85	0.44 ± 0.03	0.17

for $1 > f > f_{MO}$ [34]. In the present case however, the onset of significant conformational effects appears to be located at $f = f_1 > f_{MO}$. This point will be discussed later on.

An explanation of the red shift of the spectra by aggregation effects [29] does not make sense in the regime $1 > f > f_1$ since these would persist down to $f = 0$, while, in the present case, the trend reverses at $f = f_1$ and λ_{max} decreases with neutralization degree for $f < f_1$ (Fig. 1). In the following we argue that the initial red shift with decreasing neutralization degree can be explained by the direct effect of electrostatic interactions.

The argument is made at the level of the mean field approximation of Hückel model [17]: the interactions between π electrons are neglected and their potential energy is given by the mean field from the nuclei and the electrons in orbital other than $2p$. Then the solution of Schrödinger's equation for the system of π electrons is a linear combination of quantum states on identical sites along the polymer chain. Defining these sites is straightforward for a polyacetylene chain but becomes less obvious for a chain linking heterogeneous conjugated rings like polythiophene where even a small amount of torsion breaks the translational invariance [35]. We neglect these problems here in our very qualitative argument and assume that it is possible to obtain this solution within Hückel approximation.

To evaluate the effects of electrostatic interactions on the delocalization of π electrons we introduce then a simple electrostatic interaction potential V_{el} as:

$$V_{el}(\vec{r}) = k_B T l_B \left[\sum_{i=1}^{fN} \frac{e^{-\kappa|\vec{r}-\vec{r}_i|}}{|\vec{r}-\vec{r}_i|} - \sum_{j=1}^{(f-f_{MO})N} \frac{e^{-\kappa|\vec{r}-\vec{r}_j|}}{|\vec{r}-\vec{r}_j|} \right] \tag{3}$$

where k_B is Boltzmann's constant, T the temperature, and κ Debye's electrostatic screening parameter. The first sum in Eq. (3) corresponds to the Coulombic repulsion between a Π electron at position $\vec{r}$ and the fN COO^- groups along the chain while the second sum evaluates the Coulombic attraction between the π electrons and the $(f - f_{MO}) N$ condensed counterions with opposite charges. Uncondensed counterions in the bulk solution contribute only to Debye's screening parameter. Equation (3) has a meaning for neutralization degrees larger than f_{MO}. It estimates the strong electrostatic potential experienced by a Π electron when it comes to a position close to that of a charge. Large positive or negative values of this potential correspond to electrostatic barriers or wells that tend to localize the π electrons.

Consistently with the adiabatic approximation used in the Hückel model, the positions r_i and r_j are considered as static variables on the time scale of the π electron motion. Equation (3) should be evaluated with a realistic spatial distribution for charged groups and condensed counterions along the backbone. For annealed polyelectrolytes, this distribution is not uniform along the chains and end-effects are important [25, 26]. It is beyond the scope of the present paper to go in such details.

However the qualitative trends associated with this electrostatic potential can be obtained by an estimation of the sum in an idealized geometry: the monomers of the highly charged conjugated backbone are considered to be coplanar with the ionizable side groups alternating on each side of this rigid ribbon. The trajectory of the π electrons is pictured as a straight line at mid distance a from the alternating side groups. The distance between two ionizable groups on the same side is equal to two monomer lengths ($2b \approx 7.6$ Å) and the effects of regiorandomness are neglected. A fraction $f > f_{MO}$ of ionizable groups is set randomly in the ionized state and a fraction $f - f_{MO}$ of condensed counterions is placed randomly on these ionized sites at a distance $a + x$ from the trajectory of the π electrons. The sums in Eq. 3 can then be easily evaluated and are shown in Fig. 9 for a typical configuration and two ionic strengths. Figure 9 illustrates convincingly the spatial variations of the electrostatic potential that the π electrons
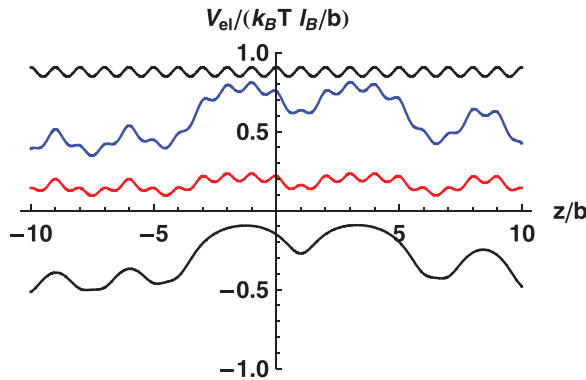
Figure 9. (color online) Evaluation of Eq. (3) for a typical random configuration of ionized sites on a rigid chain with 41 monomers with $f = 1$ and $f_{MO} = 0.54$. The electrostatic potential along the central part of the chain is displayed. The top and bottom curves display the first and second terms in Eq. (3), respectively, evaluated for $\kappa = 0.1\,\text{Å}^{-1}$. The second curve from top (blue online) is the sum of these terms. The third curve from top (red online) is the evaluation of Eq. (3) for the same configuration of ionized sites but $\kappa = 0.5\,\text{Å}^{-1}$.

have to overcome to travel along the backbone. This approach has reasonable grounds for not too large Coulombic interactions where the perturbative approach keeps a physical meaning. As these interactions increase the set of eigenstates derived in the Hückel model is no longer valid and a fully consistent solution of the Schrödinger's equation has to be found.

A quantitative estimation of the trends associated with this model can be performed by approximating the backbone as an infinite rigid line and the charges as uniform charge densities on cylindrical surfaces with a the radius of the negatively charged cylinder (COO^- groups) and a + x the radius associated to the sheath of condensed counterions. The origin is set at the position of the π electron and Eq. (3) becomes:

$$V_{el} = k_B T \frac{l_B}{b} \left[f g(\kappa, a) - (f - f_{eff}) g(\kappa, a + x) \right] \tag{4}$$

where

$$g(\kappa, d) = \frac{1}{d} \lim_{L \to \infty} \int_{-L}^{+L} \frac{\exp\left[-\kappa \left(d^2 + z^2 \right)^{1/2} \right]}{\left(d^2 + z^2 \right)^{1/2}} \, dz \tag{5}$$

is easily evaluated numerically.

Figure 10 shows the influence of neutralization degree, added salt concentration and distance of condensed counterions on the magnitude of V_{el}. The qualitative trends are in agreement with the experimental behavior. In particular the increasing number of charged groups results in a stronger electrostatic interaction with the π electrons (Figure 10, top), thus increasing their localization when $f > f_1$ (Figure 2). Added salt screens this effect (Figure 10, middle) and the conjugation length is expected to first increase upon salt addition (Figure 3). For higher salt concentrations, the decrease of λ_{max} with increasing salt concentration is linked with a different phenomenon, namely the collapse of the chains. Finally the distance of the condensed counterions to the backbone should influence the conjugation length that should decrease for bulkier counterions. We note however that dipolar interactions with ions pairs are not taken into account in our crude estimation and could also play a role. Taking the $L \to \infty$ limit in Eq. (4) is merely for convenience but does not bear a physical meaning since the conjugation length is never larger than a few tens of monomers. However the predicted qualitative trends do not depend on the length $2L$ of the rigid line and remain consistent with
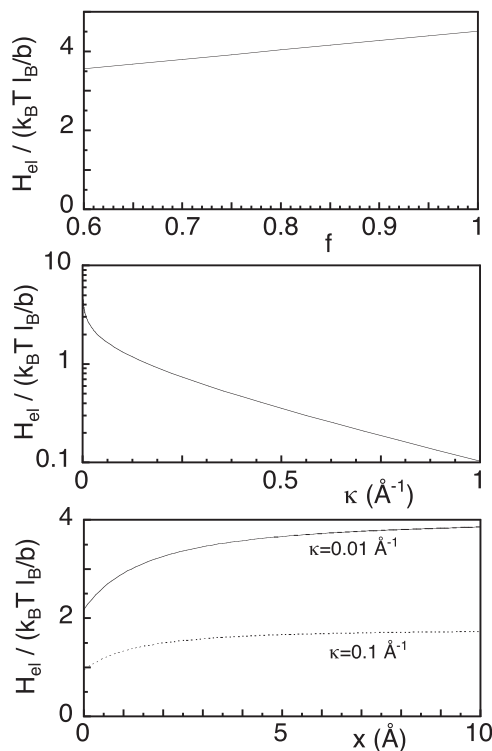
Figure 10. Influence of neutralization degree (top), screening parameter (middle) and distance of condensed counterions to the backbone (bottom) on the electrostatic perturbation of π electrons (Eq. (3)). For all the curves $a = 2$ Å and other parameters are: (top) $x = 1$ Å, $\kappa = 10^{-3}$ Å^{-1}; (middle) $f = 1$, $a = 2$ Å, $x = 1$ Å; (bottom) $f = 1$.

those obtained by the numerical evaluation of Eq. (4) for different configurations. Although localization effects are intrinsically associated with disorder effects that are not captured by uniform charge densities, estimating them with a smoothed charge distribution does not change their qualitative trends. These qualitative effects are in agreement with the experimental behavior and we conclude that the evolutions of λ_{max} and μ^2 with neutralization degree and salt concentration in the hydrophilic regime (Fig. 3) can be explained by the direct effect of Coulombic interactions on the delocalization of the π electrons. In the hydrophilic regime conformational effects play a significant role only at large salt concentrations and a blue shift is then observed for ionic strengths larger than about 0.2 mol/L (Fig. 4).

4.2. The hydrophobic regime $f < f_1$

In the regime $f < f_1$, the hydrophobicity of the polythiophene backbone is no longer largely overcompensated by the presence of charged groups: turbidity or precipitation in semi-dilute solutions can be observed for small enough neutralization degree in the presence or even in the absence of added salt. Thus we expect that the latter conditions correspond to poor solvent conditions in which isolated chains in very dilute solutions experience a collapse transition.

In the case of neutral conjugated polymers the link between the conformational disorder and the electronic states has been investigated for a long time [18, 19, 20] and increased conformational disorder is associated with a decrease in the conjugation length and the integrated

dipolar moment of transition [36]. The trends are the same when the chains experience a collapse from extended configurations to globular configurations. Therefore it is tempting to interpret the experimental behavior measured in P3TNaA solutions below f_1 along the same lines since a collapse transition is expected at small ionization degrees. As seen above, purely electrostatic effects and aggregation would yield a red shift of the absorption spectra and are not suitable explanations in this regime.

Two routes to the collapsed state of hydrophobic polyelectrolytes in water have been predicted according to the charge distribution along the chains being static or dynamic. Quenched polyelectrolytes are characterized by a static charge distribution that is frozen during the synthesis. In this case, the chains in poor solvent conditions are predicted to adopt pearl-necklace (PN) configurations, which appear as a succession of dense globules linked by stretched strings [37, 38, 39, 40, 41, 42]. As the solvent quality decreases, the fraction of monomers in the globules grows and the one in the strings diminishes.

In annealed polyelectrolytes, the charge distribution is not determined by the synthesis but each monomer is ionizable: the total charge is fixed by external parameters like the pH of the solution and the charge distribution is dynamically coupled to the conformational fluctuations [25, 43]. This coupling makes the PN configurations unstable for sufficiently poor solvent conditions [25] and a sudden transition from highly charged extended chains to weakly charged collapsed globules is predicted instead (RCSJ model) [25, 43].

The initial paper by Raphaël and Joanny [43] considers as a starting point a blob model for weakly charged quenched polyelectrolytes in a poor solvent [48]: the configuration of an isolated chain consists in a stretched chain of collapsed blobs for $\tau^{1/2}N^{-1/2}u^{-1/2} < f < \tau^{3/2}u^{-1/2}$, where $\tau = (\theta - T)/\theta$ is the reduced distance to Flory compensation temperature θ and $u = l_B/b$. For f values below this range, the electrostatic interactions become irrelevant and the chain takes a spherical globular conformation. For f values above this range, the blobs are no longer collapsed but gaussian. Scaling arguments for the electrostatic chemical potential μ_{el} in these three regimes yield [43]:

$$\begin{aligned}
\mu_{el}(f)/k_BT &\sim fu\tau^{1/3}N^{2/3}, \quad f < u^{1/2}\tau^{1/2}N^{1/2} \\
&\sim f^{-1/3}u^{1/3}\tau, \qquad \tau^{1/2}N^{-1/2}u^{-1/2} < f < \tau^{3/2}u^{-1/2} \qquad (6) \\
&\sim f^{1/3}u^{2/3}, \qquad \tau^{3/2}u^{-1/2} < f
\end{aligned}$$

Thus the electrostatic chemical potential is a non-monotonic function of f that enters the expression for the thermodynamic potential, which is minimized to obtain the equilibrium ion concentrations in the course of a potentiometric titration. Finally [43]:

$$pH \propto pK_0 + \mu_{el}(f) + k_BT \log\left[f/\left(1-f\right)\right] \qquad (7)$$

where the last term takes into account the entropy of charged groups along the chains. When the solvent is poor enough, i.e., $\tau > u^{-3/5}N^{-1/5} \approx 0.26$ here for $u = 1.87$ and $N = 125$, the non-monotonic variation of $\mu_{el}(f)$ dominates the continuous increase of the entropic term and the chemical potential $\mu(f) = \mu_{el}(f) + k_BT \log[f/(1-f)]$ becomes a non-monotonic function of the ionization degree. Triple solutions for the equation $\mu(f) = constant$ are here unphysical and only two ionization states are possible, which values are found by the Maxwell equal-area construction. If the pH is adjusted at the value of the corresponding plateau, a coexistence between collapsed weakly charged globules and charged extended chains of gaussian blobs is then expected [43].

Monte Carlo simulations provided a similar view on the transitional behavior of annealed polyelectrolytes in a poor solvent. The conformational transition upon titration of a single

freely jointed bead-spring chain was simulated by maintaining the chain in contact with a reservoir of charges with fixed chemical potential [44, 45, 46, 47]. Early results showed a continuous expansion of hydrophobic chains with increasing ionization degree [44] but more recent studies with longer chains confirmed the existence of a first-order transition that becomes smoother as the degree of polymerization decreases [45]. Moreover detailed investigations confirmed that the PN structure can be obtained only in moderately poor solvent [46, 47].

Here we are dealing with strongly hydrophobic annealed polyelectrolytes and we expect that the RCSJ model could be suited for the description of the collapse of the chains. However the presence of two IP points suggests that three successive processes occur in the titration bath as the ionization degree of the chains is decreased. In the range $f_1 > f > f_2$, the chains make the first step in their collapse with two coexisting electronic (or conformational) states of the chains, which are typical of ionization degrees $f = f_1$ and $f = f_2$. This is followed by a second step in the range $f_2 > f > f_3$, where the coexisting states correspond to $f = f_2$ and $f = f_3$. Finally in the range $f_3 > f > 0$, the absorption spectra are still evolving with λ_{max} and μ^2 monotonically decreasing but no isosbestic point can be identified. This is a far more complex behavior than predicted by theory and simulations. Therefore assigning one of these steps to the collapsed globule-extended chain transition is not an easy task.

The quantitative evaluation of the RCSJ model requires numerical front factors that are difficult to justify. The scaling laws, Eq. 6, are anchored on the estimation of the electrostatic free energy of the spherical globular conformation, $F_{el} \sim k_B T f^2 u \tau^{1/3} N^{5/3}$ [43]. This yields at least an extra front factor $\nu = 2$ in Eq. 6. With this factor, the achieving of a non-monotonic curve for $\mu(f)$ is possible only for $0.7 < \tau < 1$. Using $\nu = 5$, $\mu(f)$ is non-monotonic in the whole range $0.3 < \tau < 1$. Whatever the value of ν, however, the ionization of the collapsed state obtained from the Maxwell construction is very low, in the range 0.01–0.02, in contrast with the experimental f_i values (Table 2). This stems from the strong initial slope of $\mu_{el}(f)$, which scales as $N^{2/3}$ in the collapsed globule regime, and therefore the value of ν has only little effect on the ionization degree in the collapsed globule. On the other hand the degree of ionization in the extended state varies from about 0.07 for $\tau = 0.3$ to 0.49 for $\tau = 1$ ($\nu = 5$). Assuming rather large τ values for the conjugated backbone, it would then be tempting to identify the experimental range $f_3 < f < f_2$ with the coexistence range of globular and extended states of the chains depicted by the theory.

In the simulations typical values for the ionization of the collapsed and the extended states are respectively about 0.05 and 0.99 [45]. The latter value, which is independent of N, is considerably higher than in the theory and implies that the charged chains are fully extended [45]. Following this picture one would then associate this transition with the experimental range $f_2 < f < f_1$ as we did previously [30], since the simulations used mainly $u = 1$ and offered no possibility for counterion condensation in Manning's sense.

Clearly both possibilities leave aside one of the experimental transition ranges and are not fully satisfying. However some convergences can still be pointed out. The effects of varying N are in qualitative agreement with the expectation of a sharper transition for larger N in transition 1–2 but not in transition 2–3 (Fig. 7). However our two samples have different polydispersity indexes and this agreement should be considered with some caution. Also in agreement with both theory and simulations, the ionization in the extended state appears to be independent of N for both transitions 1–2 and 2–3 (Table 2).

The conjugation length of P3TNaA decreases with increasing temperature [12, 16]. This means that van der Waals attractions decrease and solvent quality increases at higher tem-

peratures. As a matter of fact, both transitions 1–2 and 2–3 occur at lower pH as T increases (Fig. 8).

Finally, as electrostatic screening by added NaCl increases, f_1 and f_2 tend to increase while f_3 tends to decrease (Table 2). This suggests that transition 1–2 is more concerned with electrostatic interactions than transition 2–3.

Some details in the actual interactions at work in the system could explain why the experimental behavior is not easily modeled by theory or simulations. First, the change of the solvent quality with neutralization degree is usually not considered in the models, which assume a simple additivity of Coulombic interactions with the other interactions affecting the backbone. However the hydration shell of the monomers depends on their neutralization state. Thus with lowering pH the solvent becomes poorer for the chains and τ is increasing. Second, carboxylic acids have been known for a long time for their ability to form together hydrogen bonds that affect the solubility of weak polyacids at low pH [49]. Again this would increase the τ parameter at low pH. It is not straightforward to include this effect in the RCSJ model: a simple phenomenological attempt to replace τ by $\tau' = \tau + \beta(1 - f)^2$ in the scaling expression for the free energy of the RCSJ model did not result in an increased stability of the globular state and in larger f values for the collapsed state in equilibrium with stretched chains [30].

Taking into account the above remarks, two scenarios can be imagined for the collapse of the chains, depending on the emphasis being put on the consistency with the results of either simulations or RCSJ model. In the first scenario [30], transition 1–2 is the first order collapse transition predicted by RCSJ model and simulations while transition 2–3 corresponds to a further densification of the collapsed globules through hydrogen bonding at low neutralization degree. Alternately, the second scenario would link transition 1–2 with a local collapse of the chains transforming stretched chains into a stretched assembly of gaussian blobs and identify the first order collapse transition with transition 2–3. It is interesting to note that the distinction between quenched and annealed polyelectrolytes vanishes at $f = 1$ and the difference between the two types of polyelectrolytes should probably be small in the hydrophilic regime ($f > f_1$). Therefore it is not unlikely that the local chain collapse in transition 1–2 could proceed via a PN mechanism. A τ parameter that varies with neutralization degree would also facilitate such a mechanism since τ would be small at large f values, a situation where PN configurations are expected even for annealed polyelectrolytes [25, 46, 47].

We feel that the first scenario is more realistic because it can explain the non-monotonic effect of added salt on λ_{max} at a given f (Fig. 3). Indeed, when $f \geq 0.55$ or $f \leq 0.3$, the addition of salt increases λ_{max}, while it has the reverse effect when $0.55 \geq f \geq 0.3$. As discussed in section 4.1, this effect is explained by the direct effect of electrostatic interactions at large f values. When $0.55 \geq f \geq 0.3$ added salt facilitates the collapse of the chains in the hydrophobic regime. When $f \leq 0.3$, the hydrotropic effect of added salt hinders H-bonding in the solutions and could decrease the densification of the collapsed globules at low pH. Again we emphasize that this increase of λ_{max} with added salt for $f \leq 0.3$ is not due to chain aggregation, which would be detected by an increase in the baseline level at wavelengths larger than 600 nm. For all the spectra recorded at moderate salt concentrations, the baseline remained the same during the whole titration, contrarily to what is observed when $C_{NaCl} \geq 0.2\ M$.

Further work is needed to clarify the mechanisms of transitions 1–2 and 2–3 but is not straightforward since a structural study by scattering techniques is very difficult in the very dilute regime needed to prevent phase separation. Even fluorescence correlation spectroscopy with labeled chains seems to lack the spatio-temporal resolution needed to distinguish between these two scenarios [50, 51]. In fact UV-visible spectroscopy appears to be the

technique with the highest sensitivity to the local conformation of the chains and it is difficult to check its results against those brought by less sensitive techniques. Therefore the more practical test of our conjectures could be the use of UV-visible spectroscopy in well-chosen conditions, e.g., in the presence of hydrogen bonding quenchers or hydrotropic components. Such directions will be explored in the future.

Finally we want to discuss the transition between the hydrophilic and the hydrophobic regimes, which was set to $f = f_1$ based on the non-monotonic behavior of λ_{max} and μ^2 with neutralization degree. From the discussion of these two regimes it seems clear that the mechanisms at work do not switch on and off at $f = f_1$ and that both conformational effects and direct electrostatic interactions are effective in a broader f range. Therefore $f = f_1$ is merely the value where the opposite trends associated with these two mechanisms compensate. This inversion point in the evolution of the optical properties of the chains is not necessarily identical to the compensation point of hydrophobic and electrostatic interactions. However it turns out that $f = f_1$ is also a very good approximation of this compensation point since the linear decomposition of the spectra is effective with $f = f_1$ as a reference state. The fact that $f_1 > f_{MO}$ is consistent with recent finding that the Manning-Oosawa threshold is not well defined for hydrophobic polyelectrolytes [52] and that adding charges beyond f_{MO} makes a difference for hydrophobic polyelectrolytes. It supports further the idea that hydrophobic and electrostatic effects are not simply additive, or, in terms of current models, that the reduced temperature τ depends in some way of the neutralization degree f.

To conclude, we have investigated the optical properties of an annealed hydrophobic conjugated polyelectrolyte as a function of its neutralization degree. The spectral shift, as quantified by the position of the absorption maximum, is non-monotonic as a function of the neutralization degree. From the characteristics of the UV-visible absorption spectra, we can distinguish a hydrophilic regime and a hydrophobic regime. In the hydrophilic regime the spectral shift can be explained qualitatively by dominant direct electrostatic interactions between the charges along the backbone and the Π electrons without significant conformational effects. In the hydrophobic regime, conformational effects dominate the spectral shift and two successive isosbestic points can be identified as the neutralization degree decreases. This allows us to distinguish three distinct processes in the collapse of the chains, with two of them characterized by a coexistence of two distinct conformations in a range of neutralization degrees (or pH values). We have proposed for the collapse of the chains two possible scenarios, which are waiting yet for a definitive experimental check. The P3TNaA appears to be a model system in the sense where aggregation effects appear to play no visible role in the experimental conditions investigated here. This allows us to uncover very interesting phenomena that could both play a role in the fluorescence spectroscopy of these polymers and call for a refinement of the current models of hydrophobic polyelectrolytes.

Acknowledgments

References

[1] Bhattacharjee, H. R., Preziosi, A. F., & Patel, G. N. (1980). *J. Chem. Phys.*, *73*, 1474.

[2] Patil, A. O., Ikenoue, Y., Wudl, F., & Heeger, A. J. (1987). *J. Am. Chem. Soc.*, *109*, 1858.

[3] Chen, L., McBranch, D. W., Wang, H., Helgeson, R., Wudl, F., & Whitten, D. G. (1999). *Proc. Natl. Acad. Sci. U.S.A.*, *96*, 12287.

[4] Achyuthan, K. E., Bergstedt, T. S., Chen, L., Jones, R. M., Kumaraswamy, S., Kushon, S. A., Ley, K. D., Lu, L., McBranch, D., Mukundan, H., Rininsland, F., Shi, X., Xia, W., & Whitten, D. G. (2005). *J. Mat. Chem.*, *15*, 2648.

[5] Ambade, A. V., Sandanaraj, B. S., Klaikherd, A., & Thayumanavan, S. (2007). *Polym. Int.*, *56*, 474.

[6] Herland, A., & Inganäs, O. (2007). *Macromol. Rapid Commun.*, *28*, 1703.

[7] Wang, J., Wang, D., Miller, E. K., Moses, D., Bazan, G. C., & Heeger, A. J. (2000). *Macromolecules*, *33*, 5153.

[8] Xu, Q.-H., Gaylord, B. S., Wang, S., Bazan, G. C., Moses, D., & Heeger, A. J. (2004). *Proc. Nat. Acad. Sci. U.S.A.*, *101*, 11634.

[9] Cabarcos, E. L., & Carter, S. A. (2005). *Macromolecules*, *38*, 10537.

[10] Jiang, H., Zhao, X., & Schanze, K. S. (2007). *Langmuir*, *23*, 9481.

[11] Fave, J. -L., & Schott, M. (1992). *J. Chim. Phys.*, *89*, 931.

[12] Vallat, P. (2006). Thèse Université Louis Pasteur: Strasbourg.

[13] Vallat, P., Catala, J. -M., Rawiso, M., & Schosseler, F. (2007). *Macromolecules*, *40*, 3779.

[14] Yoshino, K., Hayashi, S., & Sugimoto, R. (1984). *Jpn. J. Appl. Phys.*, *23*, L899.

[15] Sugimoto, R., Takeda, S., Gu, H. B., & Yoshino, K. (1986). *Chem. Express*, *1*, 635.

[16] Kim, B., Chen, L., Gong, J. P., & Osada, Y. (1999). *Macromolecules*, *32*, 3964; (2000). *Macromolecules*, *33*, 648.

[17] Atkins, P. W. (1990). *Physical Chemistry* 4th Edition; Oxford University Press: Oxford, UK.

[18] Patel, G. N., Chance, R. R., & Witt, J. D. (1978). *J. Polym. Sci.*, *16*, 607.

[19] Lim, K. C., & Heeger, A. J. (1985). *J. Chem. Phys.*, *82*, 522.

[20] Rawiso, M., Aimé, J. -P., Schott, M., Fave, J. -L., Schmidt, M., Muller, G., & Wegner, G. (1988). *J. Phys. Paris*, *49*, 861.

[21] de Gennes, P. G., Pincus, P. A., Velasco, R. M., & Brochard, F. (1976). *J. Phys. Paris*, *37*, 1461.

[22] Cotton, F. A., & Wilkinson, G. (1962). *Advanced Inorganic Chemistry*, 3rd edition; Wiley Interscience: New York, USA.

[23] McCullough, R. D., Ewbank, P. C., & Loewe, R. S. (1997). *J. Am. Chem. Soc.*, *119*, 633.

[24] Jost, P., Galand, N., Schurhammer, R., & Wipf, G. (2001). *Phys. Chem. Chem. Phys.*, *4*, 335.

[25] Castelnovo, M., Sens, P., & Joanny, J. -F. (2000). *Eur. Phys. J. E*, *1*, 115.

[26] Zito, T, & Seidel, C (2002). *Eur. Phys. J. E*, *8*, 339.

[27] Pinto, M. R., Kristal, B. M., & Schanze, K. S. (2003). *Langmuir*, *19*, 6523.

[28] Fan, Q.-L., Zou, Y., Lu, X.-M., Hou, X.-Y., & Huang, W. (2005). *Macromolecules*, *38*, 2927.

[29] Gao, Y., Wang, C.-C., Wang, L., & Wang, H.-L. (2007). *Langmuir*, *23*, 7760.

[30] Vallat, P., Catala, J. -M., Rawiso, M., & Schosseler, F. (2008). *Europhys. Lett.*, *82*, 28009.

[31] Brédas, J. L., Thémans, B., Fripiat, J. G., André, J. M., & Chance, R. R. (1984). *Phys. Rev. B*, *29*, 6961.

[32] Oosawa, F. (1971). *Polyelectrolytes*, Marcel Dekker: New York, USA.

[33] Manning, G. S. (1974). In *Polyelectrolytes*, Sélégny, E., Mandel, M., & Strauss, U. P. (Eds.), D. Reidel: Dordrecht, Holland.

[34] Barrat, J. -L., & Joanny, J. -F. (1996). *Adv. Chem. Phys.*, *94*, 1.

[35] Brédas, J. L., Street, G. B., Thémans, B., & André, J. M. (1985). *J. Chem. Phys.*, *83*, 1323.

[36] Soos, Z. G., & Schweizer, K. S. (1987). *Chem. Phys. Lett.*, *139*, 196.

[37] Dobrynin, A. V., Rubinstein, M., & Obukhov, S. P. (1996). *Macromolecules*, *29*, 2974.

[38] Micka, U., Holm, C., & Kremer, K. (1999). *Langmuir*, *15*, 4033.

[39] Lyulin, A. V., Dunweg, B., Borisov, O. V., & Darinskii, A. A. (1999). *Macromolecules*, *32*, 3264.

[40] Chodanowski, P., & Stoll, S. (1999). *J. Chem. Phys.*, *111*, 6069.

[41] Micka, U., & Kremer, K. (2000). *Europhys. Lett.*, *49*, 189.

[42] Deserno, M. (2001). *Eur. Phys. J. E*, *6*, 163.

[43] Raphaël, E., & Joanny, J. -F. (1990). *Europhys. Lett.*, *13*, 623.

[44] Sassi, A. P., Beltrán, S., Hooper, H. H., Blanch, H. W., Prausnitz, J., & Siegel, R. A. (1992). *J. Chem. Phys.*, *97*, 8767.

[45] Uyaver, S., & Seidel, C. (2003). *Europhys. Lett.*, *64*, 536.

[46] Uyaver, S., & Seidel, C. (2004). *J. Phys. Chem. B*, *108*, 18804.

[47] Ulrich, S., Laguecir, A., & Stoll, S. (2005). *J. Chem. Phys.*, *122*, 094911.

[48] Khokhlov, A. (1980). *J. Phys. A*, *13*, 979.
[49] Eliassaf, J., & Silberberg, A. (1962). *Polymer*, *3*, 555.
[50] Pristinski, D., Kozlovskaya, V., & Sukhishvili, S. A. (2005). *J. Chem. Phys.*, *122*, 014907.
[51] Wang, S., Zhao, J. (2007). *J. Chem. Phys.*, *126*, 091104.
[52] Essafi, W., Lafuma, F., Baigl, D., & Williams, C. E. (2005). *Europhys. Lett.*, *71*, 938.
[53] Stevens, M. J., & Kremer, K. (1995). *J. Chem. Phys.*, *103*, 1669.